Physica B 647 (2022) 414386

Contents lists available at ScienceDirect

Physica B: Physics of Condensed Matter

journal homepage: www.elsevier.com/locate/physb

# Nanoarchitectonics of n-type organic semiconductors polymerized by Cu (0)-mediated RDRP of acrylates based monomers

Ghasem Moghadam [a], Farhad Banisharif [b], Dania Ali [c], Ali H. Reshak [d,e,*], Muhammad M. Ramli [e]

[a] Department of Chemistry, University of Isfahan, 81746-73441, Isfahan, Iran
[b] School of Chemical, Petroleum and Gas Engineering, Iran University of Science and Technology, 16846-13114, Narmak, Tehran, Iran
[c] Faculty of Medicine, Charles University, Pilsen, 30100, Czech Republic
[d] Physics Department, College of Science, University of Basrah, Basrah, 61004, Iraq
[e] Center of Excellence Geopolymer and Green Technology (CEGeoGTech), University Malaysia Perlis, 01007, Kangar, Perlis, Malaysia

ARTICLE INFO

*Keywords:*
DFT calculation
Acrylates-based polymer
n-type organic semiconductors
$Cu^0$-RDRP

ABSTRACT

Metal silicates, obtained from abundant components in Earth's crust, could offer desirable activity and selectivity in catalytic applications. In this study, density functional theory (DFT), time-dependent DFT (TD-DFT), and Hartree-Fock (HF) calculations were employed to compute specified features of acrylates-based n-type organic semiconductors synthesized by copper(0)-mediated reversible deactivation radical polymerization ($Cu^0$-RDRP). After performing the molecular optimization, particular features of the synthesized semiconductor structure were captured including IR, $^1H$ and $^{13}C$ NMR, and UV–visible spectra, TDOS spectrum, HOMO and LUMO patterns, and energy gap. Lastly, the contour electron density surface (ESP) and molecular electrostatic potential (MEP) plots were also computed utilizing the gauge independent atomic orbital (GIAO) approach. These analyses reveal existence of an electron cloud around the semiconductor. The role of atomic charge for the transmission of electrons has been well shown in changing cloud charge around the acrylate monomer after polymerization as well as in changing the negative charge from organic to inorganic area in the polymer. According to these analyses, well-agreeable compatibility was attained with by comparing our theoretical simulation data on the acrylate-based n-type organic semiconductors and the reported experimental results in literature.

## 1. Introduction

Reversible inactivation radical polymerization (RDRP) techniques have opened up a new horizon to synthesize supramolecular materials possessing narrow molecular weight distribution (MWD) and high group fidelity with a specific structure and molecular weight [1]. Out of plenty of polymerization techniques, recently emerged RDRP by metallic copper ($Cu^0$), namely $Cu^0$-RDRP, has significantly contributed to the filed progress [2,3]. $Cu^0$-RDRP is a robust methodology to successfully polymerize acrylates, styrene, acrylamides, and acrylates (methyl). By utilizing $Cu^0$-RDRP, synthesis of many supramolecular polymers is facilitated, with which the final polymer group performance is maintained at high conversion. Hence, this protocol is stunningly beneficial for preparing block copolymers. Moreover, $Cu^0$-RDRP provides accessibility to several low-diffusion polymer degree index (PDI) materials using a low-cost and straightforward experimental pathway [4–6]. It also leads to obtain specific materials with low PDI and causes to substantially decrease in the amount of monomer remaining at the end of the reaction. Interestingly, around 90% and above conversions values are quantitatively reported for chain viability during $Cu^0$-RDRP reactions, wherein either high-value monomers are used, or a monomer should be excluded from the reaction [7]. Worthwhile to mention that polymeric compounds made of expensive monomers, which are rendered by this protocol through a multi-step synthesis and meticulous refining experiments, have broad and significant usage in organic electronics [8]. Plenty of these polymers, especially suitable for plastic electronics, consist of an all-carbon backbone linear chain and attached side chains of bonded pendants [9]. Amongst, supramolecular co-block polymers are even more desirable candidates to be made by $Cu^0$-RDRP polymerization. Conspicuously, the high cost of monomers and the complicated removal of remaining monomers with similar solubility compared to the formed polymers reiterate the process significance [10].

Out of many suitable polymeric monomers for the RDRP process, a

* Corresponding author. Physics Department, College of Science, University of Basrah, Basrah, 61004, Iraq.
*E-mail address:* maalidph@yahoo.co.uk (A.H. Reshak).

https://doi.org/10.1016/j.physb.2022.414386
Received 13 July 2022; Received in revised form 17 September 2022; Accepted 29 September 2022
Available online 3 October 2022

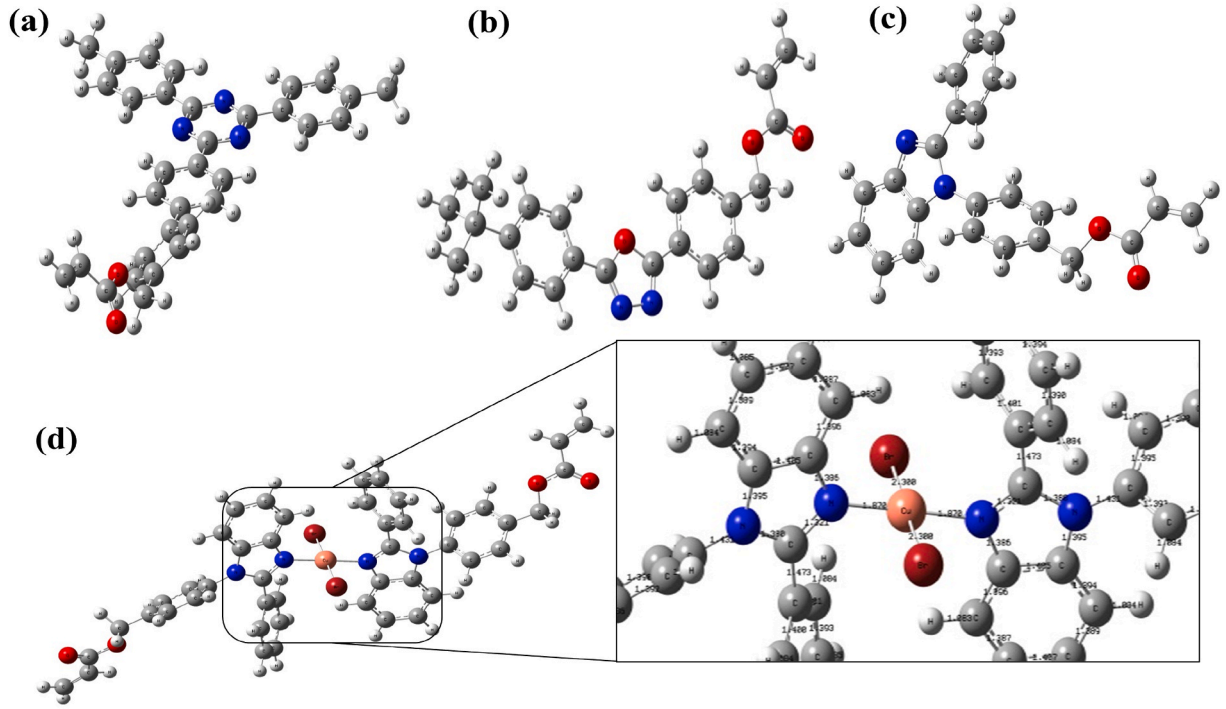


**Fig. 1.** The optimization of compounds obtained by DFT/B3LYP method and 6-311G(d,p): a) Comp-1, b) Comp-2, c) Comp-3, and d) Comp-4. Note: highlighted section shown in panel (d) of Comp-4 is to compare the N–C bond length of imidazole groups connected to Cu.

unique one is acrylic monomers [11]. Recently, acrylic-based n-type organic semiconductors were synthesized by using the modified $Cu^0$-RDRP process and were comprehensively characterized by different methods to study their pivotal features (e.g., optical properties). Such semiconductor is an essential part for many high-tech devices and advanced instruments, such as organic light-emitting diodes and some types of organic thin-film transistors. Along this line, $Cu^0$-RDRP polymerization method is tremendously assistive in producing high stable acrylates-based polymers with narrow PDI values ranging from 1.14 to 1.39. Therefore, such materials with efficient optical properties are known to be highly demanded as high-tech optoelectronics [12].

Besides experimental studies, the density functional theory (DFT) method is used as a powerful gadget to study the electronic structure of nanostructured materials at atomic level. By employing the DFT method and considering electron correlation, FT-IR vibration analysis is relatively determined and comparisons with experimental analysis on large organic molecules are carried out [13–15]. Very few studies used DFT calculation to describe the observed phenomena during the experimental studies. For example, Tonge et al. [11] used DFT function theory at B3LYP method and 6-31G+(d) basis set to calculate the high occupied molecular orbital (HOMO) energy, energetically low-lying low unoccupied molecular orbital (LUMO), HOMO-LUMO levels, and transition state for the n-type organic semiconductors with acrylate-based monomer polymerized by $Cu^0$-RDRP method. Sauve et al. [6] applied DFT to calculate ground-state geometries and energies of the acrylate-based semiconductors. Christopherson et al. [12] employed DFT calculation and the hybrid functions (B3LYP method and 6-31G+(d) and LANL2DZ ECP basis set) as a supplement to their experimental work to simulate the properties of phosphorescent iridium-containing acrylic monomers synthesized by $Cu^0$-RDRP polymerization method at room temperature. In their study, the properties of the polymer were calculated by considering the ground-state geometries and energies.

Relying on electron-deficient heterocyclic motifs, Tonge et al. [11] synthesized three derivatives of n-type acrylate-based monomers including 2,2′,2"-(1,3,5-benzinetriyl)-tris(1-phenyl-1-HPolymer benzimidazole (TPBI), 3-(biphenyl-4-yl)-5-(4-*tert*-butylphenyl)-4-phenyl-4H-1,2,4-triazole (TAZ), and Triphenyltriazines which are also highly popular amongst organic electronics. In this study and as shown in Fig. 1, they are named as compound 1 (Comp-1), compound 2 (Comp-2), and compound 3 (Comp-3), respectively. Based on the Tonge et al. study, Comp-3 exhibited the best performance for $Cu^0$-RDRP polymerization and hence is the basic polymer unit of derived complex illustrated as compound 4 (Comp-4).

In the present study, DFT calculation was employed to investigate the optimized molecular structure and energy as well as Fourier transform infrared spectroscopy (FTIR) analysis diagram of the presented Comp-1 to Comp-4. In addition, the electron density surface (ESP) and molecular electrostatic potential (MEP) plots were sketched and then employed for calculating the cloud electron mass surface that clearly determines the charge mass of the structure and each atom behavior. Subsequently, the nuclear magnetic resonance spectroscopy (NMR) of polymeric acrylate-based n-type organic semiconductors was verified under optimized conditions. Ultimately, other imperative physicochemical characterizations of the polymer have been studied by determining HOMO and LUMO, bond lengths and angles, and other electronic features such as the charge of atoms, electron affinity, and chemical potential of the polymer.

## 2. Computational details

In the present work, the Gaussian 09 W software was employed to perform density functional theory (DFT), time-dependent DFT (TD-DFT), and Hartree-Fock (HF) calculations insights [16]. The molecular structure optimization carried out via HF and DFT methods using B3LYP functional and basis sets of 6–31G(d,p) and 6-311G(d,p) to get the closest structure. Subsequently, IR and UV–visible spectra, HOMO and LUMO analysis, energy gap, and molecular electrostatic potential (MEP) plots were obtained and visualized by Gauss View 06 animation option [17]. 1H NMR, and 13C NMR spectra were computed using the gauge independent atomic orbital (GIAO) approach [18,19]. Total densities of states of electron (TDOS) spectrum for the simulated compounds (denoted as Comp-1, Comp-2, Comp-3, and Comp-4) were performed at

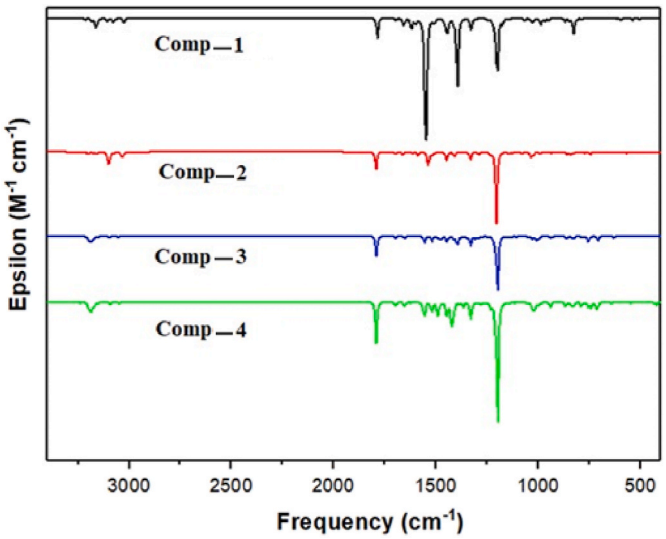


**Fig. 2.** IR spectrum of compounds carried out by B3LYP/6-311G(d,p).

GaussSum 3.0 software.

## 3. Results and discussion

### 3.1. Molecular structures

According to Tonge et al. [11] single crystals of Comp-4 was suitable for X-ray crystallography. The structure shows the CuBr2 centre adopting a square planar geometry between two benzimidazole moieties, with typical Cu–N bond lengths of 1.965 Å in the $P2_1/c$ space group.

In this study our calculation reveals that this subject as well as with closely bond length and optimization structure shown the stable backbone a square planar geometry between two benzimidazole moieties with typical Cu–N bond.

The results of optimized Comp-1 to Comp-4 obtained by the DFT/B3LYP method and 6-311G(d,p) are illustrated in Fig. 1. For the preparation of Comp-4 (complex structure), first, the comp-3 and $CuBr_2$ as Cu structure were optimized separately by B3LYP/6-311G(d,p). Then, both optimized compounds were appended to each other, and the resultant design (comp-4) was again optimized using B3LYP/6-311G(d,p). According to the highlighted section of Comp-4 (i.e., the Cu-complexed structure) illustrates in Fig. 1, the length of two N–C bonds of imidazole groups that are connected to copper from both sides, are 1.38 Å and 1.32 Å for one end and 1.38 Å and 1.43 Å for the other end. Revealed by our DFT calculation, it is inferred that the N–C bond elongates towards Cu as a result of comparing the length of same bonds in this structure. That is, Cu accepts electrons to its valence orbitals from Comp-3, which is an excellent electron-donor, to form the Cu complex compound (i.e., Comp-4) and make a stronger bond.

### 3.2. Spectroscopic characteristics

#### 3.2.1. IR spectra

The IR spectrum is one of the most popular methods to determine the structures in a chemical compound. For many years scientists and researchers in DFT calculations get Raman spectra usually performed using B3LYP functional with different basis sets [20–22]. In this study, the IR spectra of the four compounds, carried out by B3LYP/6-311G(d,p), have been demonstrated in Fig. 2. According to the figure, structural bonds appeared in the IR spectra are as follows: C═N bond stretching at 1552 cm-1, C═O stretching at 1786 cm-1, benzylic hydrogens and aromatic hydrogens at 3026 and 3239 cm-1, respectively, and ester C–O group at 1198 cm-1.

#### 3.2.2. $^{1}H$ NMR and $^{13}C$ NMR chemical shifts

Using the computational chemistry for confirming the closest structure, the GIAO 1H and 13C NMR chemical shifts in CHCl3 are mainly calculated based on the B3LYP method with a 6-311G(d,p) basis set [11, 13]. Accordingly, 1H NMR and 13C NMR patterns were calculated for

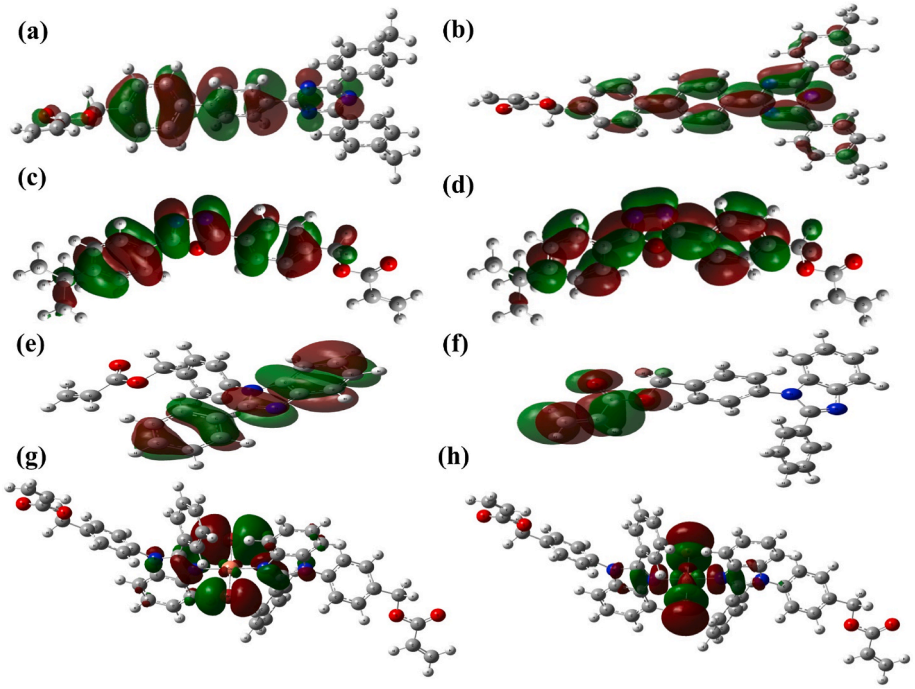


**Fig. 3.** The images of frontier orbitals, HOMO and LUMO respectively for: (a, b) Comp-1, (c, d) Comp-2, (e, f) Comp-3, and (g, h) Comp-4 (blue: nitrogen, violet: zinc, gray: carbon, red: oxygen, and white: hydrogen). (For interpretation of the references to color in this figure legend, the reader is referred to the Web version of this article.)

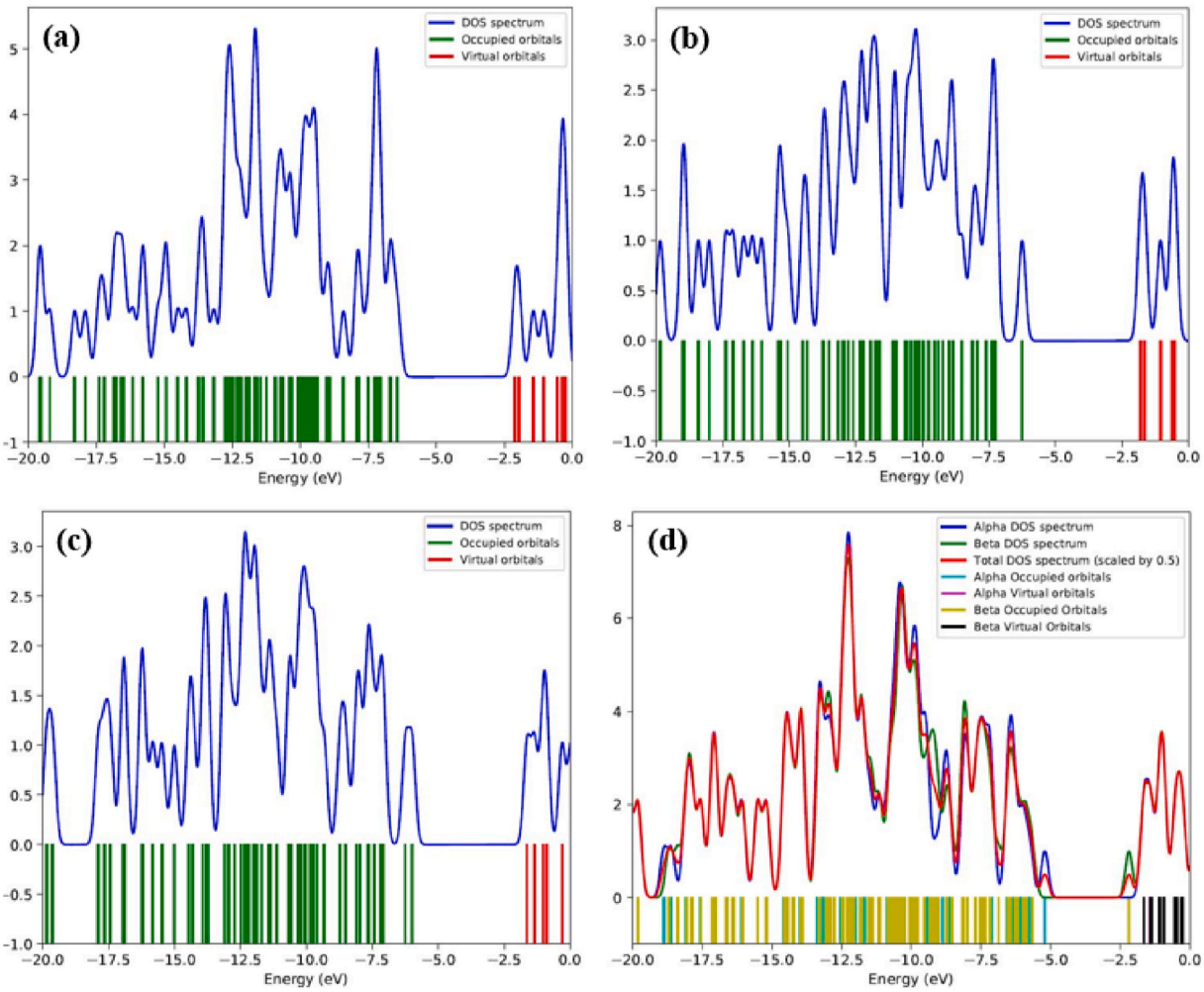


**Fig. 4.** The total densities of states (TDOS) plots of a) Comp-1, b) Comp-2, c) Comp-3, and d) Comp-4 calculated with B3LYP/6-311G(d,p) method and basis set.

Comp-3 and the result with labeling and specific atomic number for Comp-3 is carried out. (See Fig. S1 in the supporting information). In this study, with attention to experimental data [11], Comp-4 is paramagnetic and is not suitable to be analyzed by 1H or 13C NMR spectroscopy. Thus, in this study, we did not compute 1H or 13C NMR pattern for this compound. Lastly, the result demonstrates that theoretical and empirical results demonstrate a good agreement.

### 3.2.3. *UV–visible spectra*

UV visible and the electronic circular dichroism (ECD) are sensitive spectroscopy methods for analyzing the structure configuration. ECD illustrates the difference in absorption of right and left circularly polarized light related to the electronic transitions of chromophores that exist in a molecule [23–25]. According to the study reported by Tonge et al. [11], Comp-1, Comp-2, and Comp-3 have strong light absorption in the UV region of the UV–Vis spectrum. Herein, UV visible and ECD calculation based on TD-DFT with B3LYP/6-311G (d,p) method and basis set were conducted for Comp-1 to Comp-3, and the results are illustrated. (See Fig. S2 to Fig. S4 in the supporting information). Interestingly, according to this figure, absorption maxima at 280, 278, and 267 nm (for Comp-1, Comp-2, and Comp-3, respectively) reveal good agreement with experimentally reported data for UV–visible analysis [11]. Also as comparison, UV–visible of COMP-3 analysis plots calculated at ZINDO/S approach (See Fig. S5 in the supporting information).

**Table 1**
Optimization energy and some thermodynamic properties of the compounds carried out at B3LYP/6-311G(d,p) method and basis set.

| Properties | Comp-1 | Comp-2 | Comp-3 | Comp-4 |
|---|---|---|---|---|
| $E_{(Thermal)}$ (kcal/mol) | 345.819 | 263.526 | 236.389 | 479.041 |
| $C_V$ (Cal/mol. K) | 126.531 | 92.895 | 86.236 | 186.044 |
| S (Cal/mol. K) | 234.183 | 174.566 | 166.719 | 300.033 |
| HOMO (eV) | −0.23624 | −0.22972 | −0.22004 | −0.19150 |
| HOMO −1 (eV) | −0.24478 | −0.26683 | −0.22966 | −0.21096 |
| LUMO (eV) | −0.07744 | −0.06626 | −0.06024 | −0.06103 |
| LUMO +1 (eV) | −0.07205 | −0.06072 | −0.04991 | −0.06099 |
| $HLG_{ELUMO - EHOMO}$ energy gap (eV) | 0.1588 | 0.16346 | 0.1598 | 0.13047 |
| $HLG_{ELUMO+1 - EHOMO-1}$ energy gap (eV) | 0.17273 | 0.20611 | 0.17975 | 0.14997 |

### 3.3. *Frontier orbitals of HOMO-LUMO and charge distribution*

As illustrated in Figs. 3 and 4, the images of frontier HOMO and LUMO and the total densities of states (TDOS) plots for Comp-1 to Comp-4 are given. TDOS analysis is performed to further study the compatibility of examined structures according to molecular orbitals [26]. According to frontier orbitals of HOMO-LUMO and TDOS plots as completion diagram, this compound's atoms are more electronegative than the others and have the nucleophilic property. The HOMO and LUMO have strong determinative role in the chemical stability of molecules. HOMO is illustrating the capability to give electron and LUMO is

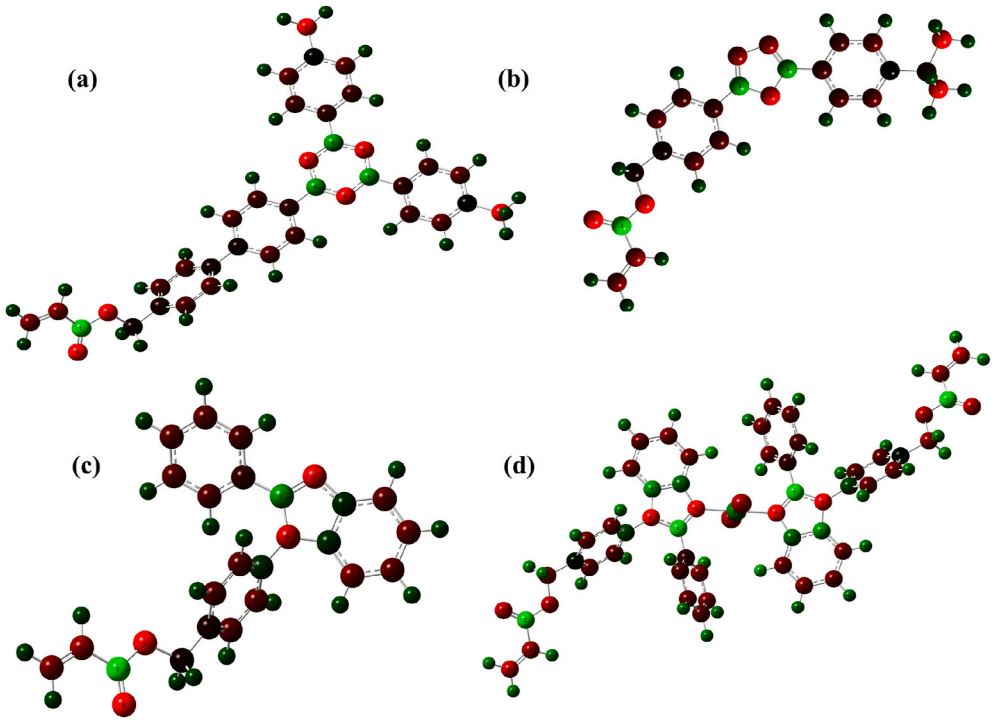


**Fig. 5.** Natural bond orbital (NBO) analysis plots based on color range corresponding to negative to positive charge distribution (red to green) for: (a) Comp-1, (b) Comp-2, (c) Comp-3, and (d) Comp-4. (For interpretation of the references to color in this figure legend, the reader is referred to the Web version of this article.)

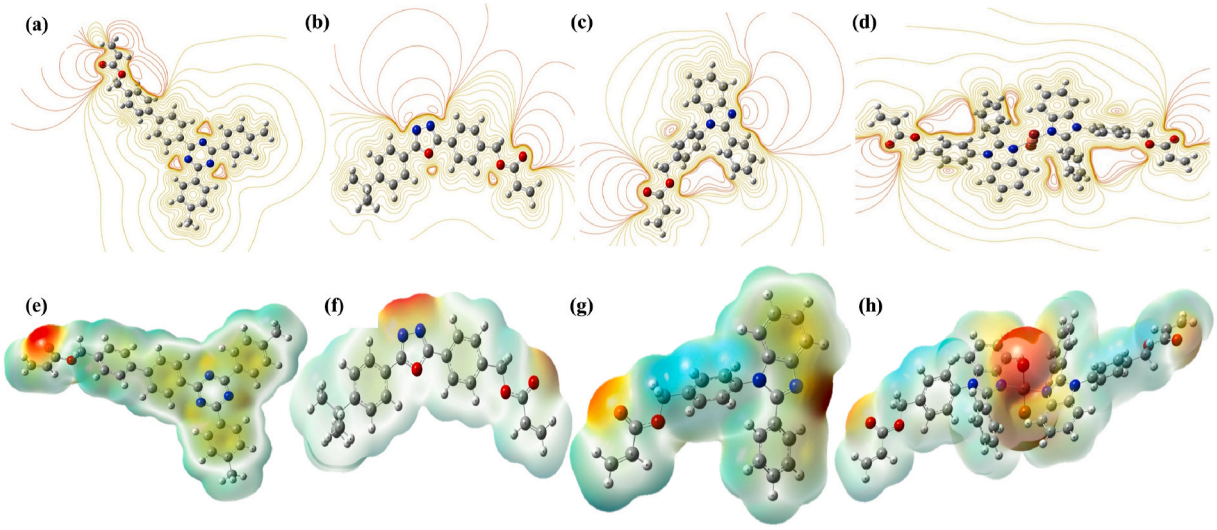


**Fig. 6.** The contour ESP plots on the left sides and the MEP plots on the right sides for: (a, e) Comp-1, (b, f) Comp-2, (c, g) Comp-3, and (d, h) Comp-4.

showing the capability to take electron. Also the energy of HOMO is directly depending on the ionization potential while the energy of LUMO is directly affiliated to electron affinity. Accordingly, optimized energy and some other thermodynamic properties computed for these compounds are listed in Table 1. According to this table and the TDOS plots, in contrast with other compounds, Comp-3 is a good nucleophile as a ligand for participating in chemical reactions for synthesizing organic semiconductors, and also Comp-4 has a good energy gap as a complex structure. Also, we reoptimized Comp-3 as the best monomer with DFT-D method and comparing specific features of the energies of system with conventional DFT and illustrated the results (See table S1 in the supporting information).

The nucleophilic, electrophilic potential, dipole moment, and interactions of molecules can be illustrated by charge distribution analysis. Not only molecular charge distribution shows dipole moment as a vector in three dimensions, but also, it is a decent approach to describe the motion of electric charges around the molecules [13]. Natural bond orbital (NBO) analysis is another critical analysis for describing molecular charge distribution [27]. Colored NBO plots are given in Fig. 5 highlighting the range of negative to positive charge distribution (by red to green) on the surface of all four compounds respectively (Fig. 5a–d). According to the plots, benzimidazoles are negative (−) regions while carbonyl groups and carbon of imidazole are positive (+) regions. Additionally, the electron density surface (ESP) and molecular electrostatic potential (MEP) plots of four compounds were employed for calculating cloud electron mass surface and represented by

the colored plot. ESP plots (Fig. 6a–d) and MEP plots (Fig. 6e–h) shown as well as benzimidazole electron area as nucleophilic group and concentration of electron density appear in nitrogen atom of imidazole. Also as comparison, Mulliken charge distribution analysis plot based on color range negative to positive (red to green) from −0.520 to 0.435 eV on the surface of Comp-3 calculated at B3LYP/6-311G (d,p) method and basis set and the result illustrated (See Fig. S6 in the supporting information).

## 4. Conclusion

In summary, In this study, HF, DFT, TD-DFT calculations were implemented to determine some specified features of acrylates-based organic semiconductors synthesized by copper(0)-mediated reversible deactivation radical polymerization ($Cu^0$-RDRP). The optimization of molecular, total densities of states of electron spectrum, IR and UV–visible spectra, HOMO and LUMO analysis, energy gap, molecular electrostatic potential plots, and $^1H$ NMR, and $^{13}C$ NMR spectra were also computed using the gauge independent atomic orbital (GIAO) method. According to this analysis, the comparison between theoretical and experimental results is in good agreement. The calculation illustrated that benzimidazoles are negative (−) region and carbonyl groups and carbon of imidazole are positive (+) region. The ESP plots shown as well as benzimidazole electron area as nucleophilic group and concentration of electron density appeared in nitrogen atom of imidazole. In contrast with other compounds, Comp-3 showed suitable nucleophilic property as a ligand for participating in chemical reactions for synthesizing organic semiconductors, and also Comp-4 represented a good energy gap as a complex structure.

## Credit author statement

**Ghasem Moghadam**: Conceptualization, Writing- Original draft preparation. **Farhad Banisharif**: Data curation, Methodology, Software, **Muhammad M. Ramli**: Visualization, Investigation. **Dania Ali**: Software, Validation.: **Ali H. Reshak**: Writing- Reviewing and Editing.

## Declaration of competing interest

The authors declare that they have no known competing financial interests or personal relationships that could have appeared to influence the work reported in this paper.

## Data availability

No data was used for the research described in the article.

## Appendix A. Supplementary data

Supplementary data to this article can be found online at https://doi.org/10.1016/j.physb.2022.414386.

## References


[1] R. Whitfield, A. Anastasaki, V. Nikolaou, G.R. Jones, N.G. Engelis, E.H. Discekici, C. Fleischmann, J. Willenbacher, C.J. Hawker, D.M. Haddleton, Universal conditions for the controlled polymerization of acrylates, methacrylates, and styrene via Cu (0)-RDRP, J. Am. Chem. Soc. 139 (2017) 1003–1010, https://doi.org/10.1021/jacs.6b11783.

[2] C.M. Tonge, F. Yuan, Z.-H. Lu, Z.M. Hudson, Cu (0)-RDRP as an efficient and low-cost synthetic route to blue-emissive polymers for OLEDs, Polym. Chem. 10 (2019) 3288–3297, https://doi.org/10.1039/C9PY00294D.

[3] G.R. Jones, R. Whitfield, A. Anastasaki, N. Risangud, A. Simula, D.J. Keddie, D. M. Haddleton, Cu (0)-RDRP of methacrylates in DMSO: importance of the initiator, Polym. Chem. 9 (2018) 2382–2388, https://doi.org/10.1039/C7PY01196B.

[4] S. Aksakal, V.P. Beyer, R. Aksakal, C.R. Becer, Copper mediated RDRP of thioacrylates and their combination with acrylates and acrylamides, Polym. Chem. 10 (2019) 6622–6629, https://doi.org/10.1039/C9PY01518C.

[5] C. Bao, J. Chen, D. Li, A. Zhang, Q. Zhang, Synthesis of lipase–polymer conjugates by Cu (0)-mediated reversible deactivation radical polymerization: polymerization vs. degradation, Polym. Chem. 11 (2020) 1386–1392, https://doi.org/10.1039/C9PY01462D.

[6] E.R. Sauvé, C.M. Tonge, N.R. Paisley, S. Cheng, Z.M. Hudson, Cu (0)-RDRP of acrylates based on p-type organic semiconductors, Polym. Chem. 9 (2018) 1397–1403, https://doi.org/10.1039/C8PY00295A.

[7] P. Mocny, H.-A. Klok, Complex polymer topologies and polymer—nanoparticle hybrid films prepared via surface-initiated controlled radical polymerization, Prog. Polym. Sci. 100 (2020), 101185, https://doi.org/10.1016/j.progpolymsci.2019.101185.

[8] E.S. Dehghani, Y. Du, T. Zhang, S.N. Ramakrishna, N.D. Spencer, R. Jordan, E. M. Benetti, Fabrication and interfacial properties of polymer brush gradients by surface-initiated Cu (0)-mediated controlled radical polymerization, Macromolecules 50 (2017) 2436–2446, https://doi.org/10.1021/acs.macromol.7b00088.

[9] S. Phan, C.K. Luscombe, Recent advances in the green, sustainable synthesis of semiconducting polymers, Trends. Chem. 1 (2019) 670–681, https://doi.org/10.1016/j.trechm.2019.08.002.

[10] C.M. Abreu, A.C. Fonseca, N.M. Rocha, J.T. Guthrie, A.C. Serra, J.F. Coelho, Reversible deactivation radical polymerization of vinyl chloride, in: Reversible Deactivation Radical Polymerization: Mechanisms and Synthetic Methodologies, ACS Publications, 2018, pp. 227–261, https://doi.org/10.1021/bk-2018-1284.ch010.

[11] C.M. Tonge, E.R. Sauvé, N.R. Paisley, J.E. Heyes, Z.M. Hudson, Polymerization of acrylates based on n-type organic semiconductors using Cu (0)-RDRP, Polym. Chem. 9 (2018) 3359–3367, https://doi.org/10.1039/C8PY00670A.

[12] C.J. Christopherson, Z.S. Hackett, E.R. Sauvé, N.R. Paisley, C.M. Tonge, D. M. Mayder, Z.M. Hudson, Synthesis of phosphorescent iridium-containing acrylic monomers and their room-temperature polymerization by Cu (0)-RDRP, J. Polym. Sci., Part A: Polym. Chem. 56 (2018) 2539–2546, https://doi.org/10.1002/pola.29233.

[13] G. Moghadam, F. Tirgir, A.H. Reshak, M. Khorshidi, Specific features of 3, 6-bis (4-hydroxy phenyl)-piperazine-2, 5-dione (BHPPD) diphenolic monomer and compered with toxic industrial bisphenol-A (BPA): DFT calculation, Mater. Chem. Phys. 236 (2019), 121780, https://doi.org/10.1016/j.matchemphys.2019.121780.

[14] F. Tirgir, M. Soleimani, G. Moghadam, M. Khorshidi, Synthesis, characterization and dehydrogenase activity of novel biodegradable nanostructure spherical shape poly (urethane-imide-sulfonamide) as pseudo-poly (amino acid) s from l-tyrosine, Polym. Bull. 75 (2018) 1055–1073, https://doi.org/10.1007/s00289-017-2074-3.

[15] G. Moghadam, J. Abdi, F. Banisharif, A. Khataee, M. Kosari, Nanoarchitecturing hybridized metal-organic framework/graphene nanosheet for removal of an organic pollutant, J. Mol. Liq. 341 (2021), 117323, https://doi.org/10.1016/j.molliq.2021.117323.

[16] M.J. Frisch, G.W. Trucks, H.B. Schlegel, G.E. Scuseria, M.A. Robb, J.R. Cheeseman, G. Scalmani, V. Barone, G.A. Petersson, H. Nakatsuji, X. Li, M. Caricato, A. V. Marenich, J. Bloino, B.G. Janesko, R. Gomperts, B. Mennucci, H.P. Hratchian, J. V. Ortiz, A.F. Izmaylov, J.L. Sonnenberg, , Williams, F. Ding, F. Lipparini, F. Egidi, J. Goings, B. Peng, A. Petrone, T. Henderson, D. Ranasinghe, V.G. Zakrzewski, J. Gao, N. Rega, G. Zheng, W. Liang, M. Hada, M. Ehara, K. Toyota, R. Fukuda, J. Hasegawa, M. Ishida, T. Nakajima, Y. Honda, O. Kitao, H. Nakai, T. Vreven, K. Throssell, J.A. Montgomery Jr., J.E. Peralta, F. Ogliaro, M.J. Bearpark, J. J. Heyd, E.N. Brothers, K.N. Kudin, V.N. Staroverov, T.A. Keith, R. Kobayashi, J. Normand, K. Raghavachari, A.P. Rendell, J.C. Burant, S.S. Iyengar, J. Tomasi, M. Cossi, J.M. Millam, M. Klene, C. Adamo, R. Cammi, J.W. Ochterski, R.L. Martin, K. Morokuma, O. Farkas, J.B. Foresman, D.J. Fox, Gaussian 16, Rev. C.01, Wallingford, CT, 2016.

[17] R. Dennington, T. Keith, J. Millam, GaussView 5 (2009).

[18] S. Jadoun, A. Verma, U. Riaz, Luminol modified polycarbazole and poly (o-anisidine): theoretical insights compared with experimental data, Spectrochim. Acta Mol. Biomol. Spectrosc. 204 (2018) 64–72, https://doi.org/10.1016/j.saa.2018.06.025.

[19] N. Singh, P. Kumar, R. Kumar, U. Riaz, Ultrasound-assisted polymerization of dyes with phenylenediamines: facile method to design polymeric photosensitizers with enhanced singlet oxygen generation characteristics and anticancer activity, Ind. Eng. Chem. Res. 58 (2019) 14044–14057, https://doi.org/10.1021/acs.iecr.9b01275.

[20] M.M. Mendes-Pinto, E. Sansiaume, H. Hashimoto, A.A. Pascal, A. Gall, B. Robert, Electronic absorption and ground state structure of carotenoid molecules, J. Phys. Chem. B 117 (2013) 11015–11021, https://doi.org/10.1021/jp309908r.

[21] T. Kupka, A. Buczek, M.A. Broda, M. Stachów, P. Tarnowski, DFT studies on the structural and vibrational properties of polyenes, J. Mol. Model. 22 (2016) 1–11, https://doi.org/10.1007/s00894-016-2969-1.

[22] A. Requena, J. Ceron-Carrasco, A. Bastida, J. Zuniga, B. Miguel, A density functional theory study of the structure and vibrational spectra of β-carotene, capsanthin, and capsorubin, J. Phys. Chem. A 112 (2008) 4815–4825, https://doi.org/10.1021/jp710304u.

[23] N. Harada, K. Nakanishi, Circular Dichroic Spectroscopy: Exciton Coupling in Organic Stereochemistry, Univ Science Books, 1983.

[24] R.W. Woody, Theory of circular dichroism of proteins, in: Circular Dichroism and the Conformational Analysis of Biomolecules, Springer, 1996, pp. 25–67.

[25] D.A. Lightner, J.E. Gurst, Organic Conformational Analysis and Stereochemistry from Circular Dichroism Spectroscopy, John Wiley & Sons, 2000.
[26] A.K. Babaheydari, A. Jafari, G. Moghadam, K. Tavakoli, Investigation and study of adsorption properties of H2S on carbon nanotube (8, 0)(SWCNT) using density functional theory calculation, Adv. Sci. Lett. 19 (2013) 3201–3205, https://doi.org/10.1166/asl.2013.5161.
[27] E.C. Vik, P. Li, P.J. Pellechia, K.D. Shimizu, Transition-state stabilization by n→ π* interactions measured using molecular rotors, J. Am. Chem. Soc. 141 (2019) 16579–16583, https://doi.org/10.1021/jacs.9b08542.